Neutron-diffraction study of the carrier-concentration-induced ferromagnet-to-spin-glass transition in the diluted magnetic semiconductor $Sn_{1-x}Mn_xTe$

C. W. H. M. Vennix and E. Frikkee
Netherlands Energy Research Foundation ECN, P.O. Box 1, 1755 ZG Petten, The Netherlands

P. J. T. Eggenkamp, H. J. M. Swagten, K. Kopinga, and W. J. M. de Jonge
Department of Physics, Eindhoven University of Technology, P.O. Box 513, 5600 MB Eindhoven, The Netherlands
(Received 17 February 1993)

In the diluted magnetic semiconductor $Sn_{1-x}Mn_xTe$ the charge-carrier concentration p is of crucial importance for the low-temperature magnetic behavior. By means of neutron-diffraction experiments, in combination with ac-susceptibility, magnetization, and specific-heat data, we show that for $x=0.04$ the long-range-ordered ferromagnetic state observed for $p=7\times10^{20}$ cm^{-3} gradually evolves into a spin-glass state with increasing carrier concentration. In a crystal with $p=11\times10^{20}$ cm^{-3} initially a transition to a restricted-ranged ferromagnetic order occurs when the temperature is lowered in zero field, followed by a transition into a reentrant spin-glass phase. By the application of a small magnetic field (5.0 mT) the reentrant spin-glass transition is suppressed. In a $p=23\times10^{20}$ cm^{-3} crystal a spin-glass phase is entered directly from the paramagnetic regime. The neutron-diffraction results indicate the presence of short-range ferromagnetic fluctuations in this sample. The results are discussed in the context of a Ruderman-Kittel-Kasuya-Yosida model. A three-dimensional (T,x,p) magnetic phase diagram is presented.

I. INTRODUCTION

Diluted magnetic semiconductors (DMS's) are ternary or quaternary alloys in which a part of the nonmagnetic cations of the host material has been substituted by magnetic ions. There is a close relationship between the magnetic and electronic properties of DMS's, resulting from the coupling between the two interacting subsystems, formed by the electronic system of the charge carriers and the diluted magnetic system of the magnetic ions, respectively.[1,2] The Mn containing IV-VI DMS's can, with respect to their magnetic properties, roughly be divided into two groups, distinguished by their charge-carrier concentrations. The first group consists of the materials with relatively low carrier concentrations, i.e., in the range $10^{17}-10^{19}$ cm^{-3}, such as $Pb_{1-x}Mn_xTe$. Their magnetic behavior closely resembles that of the Mn containing II-VI DMS's and can be ascribed to antiferromagnetic interactions of the superexchange type between the Mn ions. The existence of a spin-glass phase at low temperature has been reported for this group of materials.[3] For the second group of IV-VI DMS's, with charge-carrier concentrations of the order of 10^{21} cm^{-3}, a completely different low-temperature magnetic behavior is observed. Ferromagnetic ordering has been reported in, for example, $Sn_{1-x}Mn_xTe$ (Refs. 4–6) and $Ge_{1-x}Mn_xTe$.[7] The ferromagnetic interactions are induced by the Ruderman-Kittel-Kasuya-Yosida[8] (RKKY) indirect exchange mechanism, in which the interaction between the magnetic ions is mediated by the itinerant charge carriers.[5,7] In the case of the first group of IV-VI DMS's the carrier concentration is too small to make the RKKY interaction effective, which leads to the dominant role of the antiferromagnetic superexchange mechanism.

The crucial role of the charge-carrier concentration (p) in IV-VI DMS's becomes especially clear in the intermediate regime, with carrier concentrations of the order $10^{19}-10^{21}$ cm^{-3}. This range can be reached either by the preparation of mixed compounds such as $Pb_{1-x-y}Sn_yMn_xTe$, or by changing the carrier concentration, which actually originates from slight deviations from stoichiometry, by means of isothermal annealing. Story *et al.*[9] made the link between the antiferromagnetic and the ferromagnetic regime by the discovery of the so-called carrier-concentration-induced ferromagnetism in the compound $Pb_{0.25}Sn_{0.72}Mn_{0.03}Te$. They established the existence of a critical charge-carrier density $p_c\approx3\times10^{20}$ cm^{-3}. For $p<p_c$ paramagnetic behavior was observed down to 1.2 K, the lowest temperature covered in their experiments. Measurements of the high-temperature susceptibility yielded Curie-Weiss temperatures (Θ) equal to (0.0 ± 0.2) K. For $p>p_c$ a steplike increase of the ferromagnetic interactions, probed by a steplike increase in Θ, was observed, accompanied by a ferromagnetic ordering at temperatures below 5 K. This was a demonstration of the direct impact of the charge-carrier concentration on the magnetic phase diagram, implying the introduction of the charge-carrier concentration p as a parameter in the magnetic phase diagram, besides the temperature T and the Mn concentration x. Swagten *et al.*[10] were able to explain the influence of the carrier concentration by modifying the conventional RKKY model for the band structure of $Pb_{1-y}Sn_yTe$. In this model contributions from charge carriers in two valence bands, located in different regions of the Brillouin zone, are taken into account. When p exceeds the critical

density p_c, the Fermi level enters a set of heavy-hole valence bands, located along the Σ axis, which brings about the steplike increase of the ferromagnetic interactions. Recently Story *et al.*[11] further refined this model by the incorporation of the anisotropy and the many-valley structure of the heavy-hole Σ band.

A similar charge-carrier-concentration-induced transition to a ferromagneticlike state, indicated by measurements of the ac susceptibility, the magnetization, and the magnetic specific heat, was reported[12] for $Sn_{1-x}Mn_xTe$ with $x=0.03$ and $x=0.06$, again with $p_c \approx 3\times10^{20}$ cm^{-3}. With the aid of neutron-diffraction experiments we were able to establish the genuine ferromagnetic nature of the low-temperature phase[13] in crystals with $x=0.03$, $p=7\times10^{20}$ cm^{-3} and $x=0.06$, $p=11\times10^{20}$ cm^{-3}. In earlier reports, however, the low-temperature, high-carrier-concentration phase of $Sn_{1-x}Mn_xTe$ had not only been identified as ferromagnetic, as mentioned above, but also as a (reentrant) spin-glass phase. Mauger and Escorne[14] published a (T,x) magnetic phase diagram for $x \leq 0.06$, showing a spin-glass state at low temperatures for $x<0.03$ and a reentrant spin-glass state for $0.03<x<0.06$. The origin of these contradictory results was elucidated in a recent paper,[15] where the susceptibility, magnetization, and magnetic specific-heat experiments on $Sn_{0.97}Mn_{0.03}Te$ samples were extended to carrier concentrations as high as $p=23\times10^{20}$ cm^{-3}. A comparison with the previous results for $p=7\times10^{20}$ cm^{-3} showed that the ferromagnetically ordered state had changed into a spin-glass-like phase for the sample with $p=23\times10^{20}$ cm^{-3}. This was, to our knowledge, the first observation of a breakdown of a ferromagnetically ordered state induced by a change in the charge-carrier concentration, illustrating the decisive role of the charge-carrier density in the magnetic (T,x,p) phase diagram. To study the evolution of the magnetic correlations with increasing carrier concentration we have performed neutron-diffraction experiments on three $Sn_{0.96}Mn_{0.04}Te$ crystals with $p=7$, 11, and 23×10^{20} cm^{-3}, respectively. The experiments were combined with measurements of the ac susceptibility, the magnetization, and the magnetic specific heat. We will present evidence that with increasing charge-carrier concentration the low-temperature magnetic state gradually evolves from a ferromagnetic state for $p=7\times10^{20}$ cm^{-3}, via a reentrant spin-glass state for $p=11\times10^{20}$ cm^{-3}, into a spin-glass state for $p=23\times10^{20}$ cm^{-3}. In Sec. II of this paper the preparation of the samples will be described. The results of the measurements of the susceptibility, the magnetization, and the specific heat will be presented in Sec. III, followed by those of the neutron-diffraction experiments in Sec. IV. In the last section we will discuss our results in view of the aforementioned RKKY model. By combining the present results with those for other Mn concentrations a three-dimensional (T,x,p) magnetic phase diagram will be compiled.

II. PREPARATION

In IV-VI group semiconductors the carrier concentration is mainly determined by the number of metal and nonmetal vacancies. The first create holes, the latter create electrons. In the Sn-Te phase diagram the solidus area is completely located at the Te-rich side and consequently only p-type conductivity is observed.[16] The borders of the solidus area are situated at $Sn_{0.9996}Te$ and $Sn_{0.953}Te$, corresponding to charge-carrier concentrations of roughly 2×10^{20} cm^{-3} and 20×10^{20} cm^{-3}, respectively. By isothermal annealing in an appropriate atmosphere the number of vacancies and hence the carrier concentration can be changed.

TABLE I. Properties of the samples used in the experiments described in Sec. III. x (EPMA) is the Mn concentration determined by electron probe microanalysis. Charge-carrier concentrations were measured at 77 K. Θ and x (HTχ) were determined from the high-temperature susceptibility measurements described in Sec. III A. Except for the as-grown $p=11\times10^{20}$ cm^{-3} sample, the same samples were used for the neutron-scattering experiments.

Treatment	x (EPMA)	p (10^{20} cm^{-3})	Θ (K)	x (HTχ)
Sn annealed		7.4±0.3	7.1±0.1	4.4±0.1
As grown	4.0	11.4±0.3	7.2±0.1	4.0±0.1
$Sn_{0.57}Te_{0.53}$ annealed		23±1	7.0±0.1	4.1±0.1

Our samples were grown, using a conventional Bridgman technique, with a composition (Sn+Mn):Te=0.984, which is the equilibrium cation:anion ratio at the maximum melting temperature for SnTe. This ratio results in a carrier concentration $p \approx 10\times10^{20}$ cm^{-3}. All annealings were performed at 700 °C, lasted typically 72 h, and were followed by quenching to room temperature. The ampoules were filled with 280 mbar Ar, to guarantee a homogeneous temperature distribution, and a source material that was physically separated from the sample to be annealed. Annealing in a relatively Te-rich atmosphere, supplied by the vapor of $Sn_{0.47}Te_{0.53}$ source material, yielded carrier densities of typically 20×10^{20} cm^{-3}. Lower concentrations (typically $p \approx 5\times10^{20}$ cm^{-3}) were achieved by annealing with pure Sn as source material. The apparent carrier concentrations have been measured by the Hall effect, using the Van der Pauw method. Since p appears to be constant below 100 K,[9] we refer to the values at liquid-nitrogen temperature. The composition and the homogeneity of the samples were checked with electron probe microanalysis (EPMA). For all samples the Mn concentration was within 10% equal to the nominal concentration.

All $Sn_{0.96}Mn_{0.04}Te$ samples used in the experiments discussed in this paper were from the same Bridgman-batch. In Table I the compositions and carrier concentrations are listed.

III. RESULTS: ac SUSCEPTIBILITY, MAGNETIZATION, AND MAGNETIC SPECIFIC HEAT

A. ac susceptibility

The ac susceptibility has been measured using a mutual inductance bridge. The frequency of the 1.6 μT driving ac field was 913 Hz. In Fig. 1 the inverse of the real part of the susceptibility in the high-temperature region is displayed for the $p=7$, 11, and 23×10^{20} cm^{-3} samples.

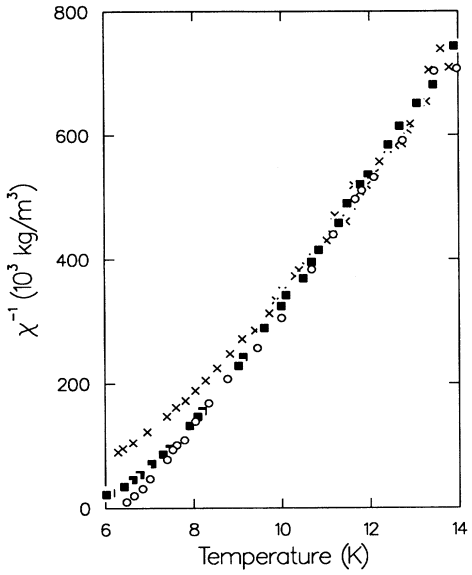

FIG. 1. Temperature dependence of the reciprocal susceptibility for $Sn_{0.96}Mn_{0.04}Te$ with $p=7\times10^{20}$ cm^{-3} (○), $p=11\times10^{20}$ cm^{-3} (■), and $p=23\times10^{20}$ cm^{-3} (×).

In all cases the data have been fitted to a Curie-Weiss law, yielding the Curie-Weiss temperatures Θ and the Mn concentrations x listed in Table I. In the fits the values $S=\frac{5}{2}$ and $g=2$ were used. All samples have a Curie-Weiss temperature of approximately 7 K. This positive value of Θ indicates that the sum of the exchange interactions, $\sum J_{ij}$, is ferromagnetic. Figure 1 shows that as the carrier concentration increases deviations from Curie-Weiss behavior occur at higher temperatures: for the $p=23\times10^{20}$ cm^{-3} sample deviations start at approximately 11 K, for $p=11\times10^{20}$ cm^{-3} at 9 K, whereas in the $p=7\times10^{20}$ cm^{-3} sample Curie-Weiss behavior is maintained until just above $T=\Theta$.

Figures 2(a) and 2(b), respectively, show the real and imaginary part of the ac susceptibility in the low-temperature region for all three samples. The data for the sample with $p=7\times10^{20}$ cm^{-3} show the characteristic features of a ferromagnetic transition. First, there is a sharp transition in both the real and the imaginary component with a critical or Curie-temperature $T_c\approx6.3$ K, which is approximately equal to the Curie-Weiss temperature Θ, and, second, the maximum value of the real component of the susceptibility is of the order of $1/N$, where N is the demagnetizing factor of the sample.

For the as-grown sample, with $p=11\times10^{20}$ cm^{-3}, the real part of the susceptibility shows a gradual increase below 6.5 K, smoothly transforming into a steep rise towards a maximum at 4.3 K. The imaginary part displays a shoulder around this temperature, but continues to increase until a maximum is reached at 2.3 K. In the real component a change of slope is seen around the same temperature. A similar behavior has been reported for a diversity of reentrant spin-glass systems, such as $Eu_xSr_{1-x}S$,[17] *Ni*Mn,[18] $(Pd_{0.9965}Fe_{0.0035})_{1-x}Mn_x$,[19] and a number of amorphous Fe-Mn and Fe-Ni alloys.[20] In these systems the sharp increase in the real part of the susceptibility is interpreted as a transition to a ferromagnetically ordered state, followed by a second transition to a spin-glass phase at lower temperature, denoted by the maximum in the imaginary part. The higher maximum in the real part of the susceptibility for the sample with $p=11\times10^{20}$ cm^{-3} compared to that with $p=7\times10^{20}$ cm^{-3} is probably related to the different dimensions of the samples.

The real component of the ac susceptibility of the $p=23\times10^{20}$ sample shows a cusplike maximum at 2.2 K, i.e., far below the Curie-Weiss temperature $\Theta=7.0$ K, ac-

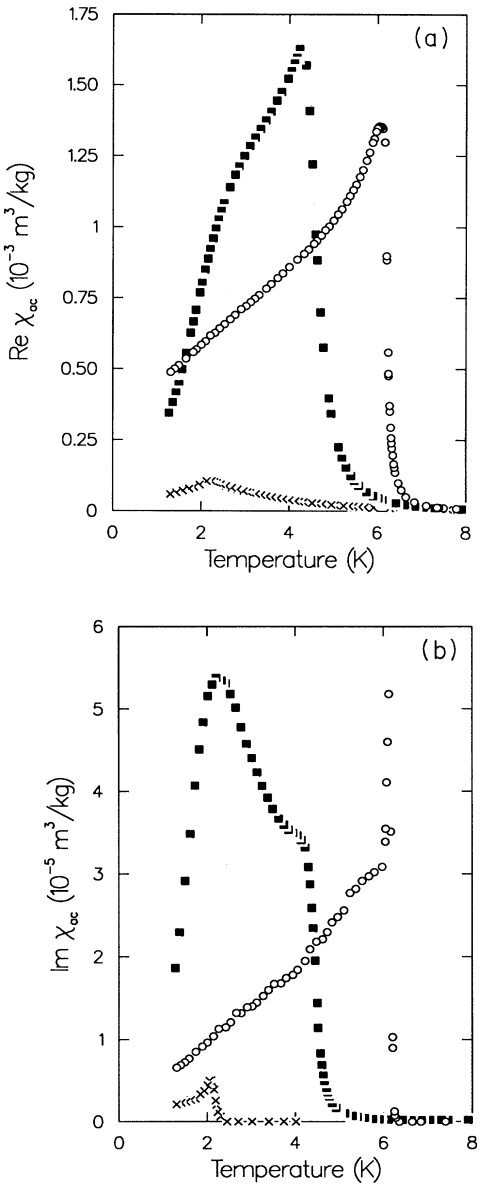

FIG. 2. Temperature dependence of the real (a) and the imaginary (b) component of the ac susceptibility for $Sn_{0.96}Mn_{0.04}Te$ with $p=7\times10^{20}$ cm^{-3} (○), $p=11\times10^{20}$ cm^{-3} (■), and $p=23\times10^{20}$ cm^{-3} (×). Driving ac field: 1.6 μT, 913 Hz.

companied by a somewhat steeper increase in the imaginary part at the same temperature. The height of the maximum in the real component does not exceed 10% of the demagnetizing limit. Both the height and the shape of the maximum in the real part indicate that the sample undergoes a transition to a spin-glass state at the freezing temperature $T_f \approx 2.2$ K.[21] The aforementioned deviations from Curie-Weiss behavior at temperatures as high as $5T_f$ (see Fig. 1), that were also reported[22] for the canonical spin-glass *Cu*Mn, support this conclusion.

We also studied the frequency dependence of the ac susceptibility. In this paper only the main results will be mentioned, more detailed results will be published separately.[23] For $p = 7\times10^{20}$ cm^{-3} there is no significant dependence on the ac frequency. For $p = 23\times10^{20}$ cm^{-3} both the maximum in the real and that in the imaginary component shift towards higher temperature and decrease in absolute value with increasing frequency. The phenomenon of a frequency-dependent freezing temperature is generally considered to be a characteristic feature of spin glasses.[24] For $p = 11\times10^{20}$ cm^{-3} the aforementioned change of slope at lower temperatures in the real component shifts towards higher temperature with increasing frequency, whereas the absolute value decreases in this temperature range. The maximum in the imaginary part tends to decrease and to move to higher temperature with increasing frequency. This indicates that also in this sample a transition to a spin-glass-like state occurs at low temperatures.

B. Magnetization

We measured the field-cooled magnetization in a 2.0 mT field for the samples with $p = 7$, 11, and 23×10^{20} cm^{-3}, using a standard vibrating sample magnetometer. The results are shown in Fig. 3. The magnetization for the sample with $p = 7\times10^{20}$ cm^{-3} rises sharply at 6.3 K, the same temperature where the ac susceptibility has its maximum slope. The shape of the curve confirms the ferromagnetic nature of the phase transition suggested by the susceptibility measurements. In the sample with $p = 23\times10^{20}$ cm^{-3} the magnetization increases more gradually with decreasing temperature and its magnitude is strongly suppressed. Of course, this behavior does not prove the existence of a spin-glass state, but it certainly reveals the collapse of the ferromagnetic state that is observed for $p = 7\times10^{20}$ cm^{-3}. The sample with $p = 11\times10^{20}$ cm^{-3} displays a temperature dependence of the magnetization which is neither ferromagnetic nor spin-glass-like. Below 6 K there is an increase in the magnetization, but less sharp than for $p = 7\times10^{20}$ cm^{-3}. With further decreasing temperature the magnetization continues to increase, until a broad maximum is reached near 2.35 K, approximately the same temperature where the imaginary part of the susceptibility has its maximum. Below this temperature the magnetization decreases. A similar behavior of the field-cooled magnetization has previously been reported[25] for the magnetic alloys *Fe*Al, *Cr*Fe, and *Au*Fe in the reentrant spin-glass concentration range.

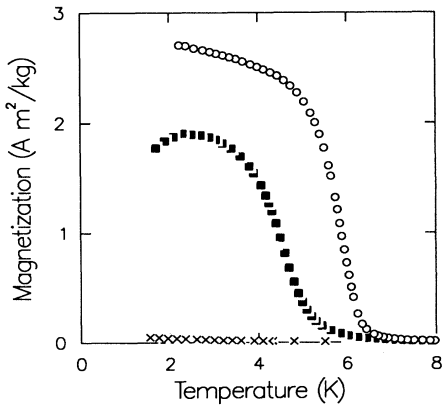

FIG. 3. Temperature dependence of the field-cooled magnetization for $Sn_{0.96}Mn_{0.04}Te$ with $p = 7\times10^{20}$ cm^{-3} (○), $p = 11\times10^{20}$ cm^{-3} (■), and $p = 23\times10^{20}$ cm^{-3} (×). $B = 2.0$ mT.

C. Specific heat

In Fig. 4 the magnetic specific heat, measured with a heat pulse calorimeter, is displayed for the samples with $p = 7$, 11, and 23×10^{20} cm^{-3}. The magnetic part of the specific heat was obtained by subtracting the lattice specific heat, i.e., the measured specific heat of the host material SnTe, from the raw $Sn_{1-x}Mn_xTe$ data. For the sample with $p = 7\times10^{20}$ cm^{-3}, a λ anomaly, characteristic for a second-order transition, is observed at the critical temperature. With increasing charge-carrier concentration this anomaly gradually transforms into a broad maximum for $p = 23\times10^{20}$ cm^{-3}. The curve for the sample with $p = 11\times10^{20}$ cm^{-3} still has a distinct maximum near the temperature where the real part of the susceptibility has a maximum, but for $p = 23\times10^{20}$ cm^{-3} no special feature is observed at the freezing temperature T_f, where the cusp in the ac susceptibility occurs. Such a smooth temperature dependence of the magnetic specific heat, without a distinct anomaly at T_f, is also observed

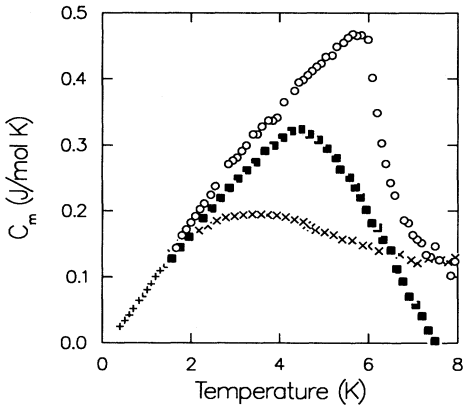

FIG. 4. Temperature dependence of the magnetic specific heat for $Sn_{0.96}Mn_{0.04}Te$ with $p = 7\times10^{20}$ cm^{-3} (○), $p = 11\times10^{20}$ cm^{-3} (■), and $p = 23\times10^{20}$ cm^{-3} (×), and for $Sn_{0.97}Mn_{0.03}Te$ with $p = 23\times10^{20}$ cm^{-3} (+). The data for $x = 0.03$ have been scaled to $x = 0.04$.

for archetypical spin glasses such as *Cu*Mn.[26]

Another indication for the existence of a spin-glass state at low temperatures for this range of carrier concentrations and Mn concentrations is found for $Sn_{1-x}Mn_xTe$ with $x=0.03$ and $p=23\times10^{20}$ cm^{-3}. Above 1.5 K a qualitatively similar behavior of the magnetic specific heat is found as for the 4% Mn sample with $p=23\times10^{20}$ cm^{-3} discussed above.[15] New data, in the temperature range down to 0.2 K, are included in Fig. 4 after scaling to $x=0.04$. They show an approximately linear temperature dependence of the magnetic specific heat, extrapolating to an intersection of the temperature axis at 0.17 K. This positive intersection as well as the proportionality with temperature are considered to be typical spin-glass features.[27]

An analysis of the magnetic entropy shows that for the samples with $p=7\times10^{20}$ cm^{-3} and $p=23\times10^{20}$ cm^{-3} the total magnetic entropy S_m that is recovered in the temperature range up to 10 K is approximately equal to the theoretical value $S_m=xR\ln(2S+1)$, with $x=0.04$ and $S=\frac{5}{2}$. In the sample with $p=11\times10^{20}$ cm^{-3} the experimentally observed entropy amounts only to about 80% of the theoretical value. When the entropy recovered below the temperatures where the real component of the susceptibility shows a maximum is compared to the total theoretical entropy, it appears that 83% is gained below 6.1 K in the sample with $p=7\times10^{20}$ cm^{-3}. This is in good agreement with the theoretical value for a three-dimensional fcc Heisenberg ferromagnet.[28] In the $p=11\times10^{20}$ cm^{-3} sample 63% is recovered below 4.3 K. In the sample with $p=23\times10^{20}$ cm^{-3} only about 35% of the theoretical entropy is recovered below 2.2 K. This result is in good agreement with that of Wenger and Keesom[26] for the spin glass *Cu*Mn.

D. Provisional conclusions

The results of the measurements of the ac susceptibility, the magnetization, and the magnetic specific heat on the $Sn_{0.96}Mn_{0.04}Te$ samples with $p=7$, 11, and 23×10^{20} cm^{-3} strongly suggest a carrier-concentration-induced breakdown of a ferromagnetic state to a spin-glass state. For the sample with the lowest carrier density a transition to a ferromagnetic ordered state at $T_c=6.3$ K is indicated by the sharp increase in the susceptibility, the presence of a spontaneous magnetization, and the λ anomaly in the specific heat. For the intermediate carrier concentration $p=11\times10^{20}$ cm^{-3} the results suggest the existence of a reentrant spin-glass phase. With lowering temperature initially a transition to a ferromagnetic state occurs at 4.5 K, indicated by the increase in the real part of the ac susceptibility and in the spontaneous magnetization. A second transition, to a spin-glass phase, takes place at 2.3 K, signaled by the maximum in the imaginary part of the ac susceptibility and the decrease in the spontaneous magnetization. The data for the sample with $p=23\times10^{20}$ cm^{-3} strongly suggest a transition to a spin-glass state at the freezing temperature $T_f=2.2$ K, identified by the cusp in the ac susceptibility, the absence of a spontaneous magnetization, and the smooth temperature dependence of the specific heat.

Although suggestive, most of the evidence presented above is somewhat circumstantial. To obtain convincing evidence for the conjectured collapse of the ferromagnetic state with increasing charge-carrier concentration we started neutron-scattering experiments. With the aid of neutron diffraction it is not only possible to gain insight in the *nature* of the magnetic ordering, but also in the *range* of the magnetic correlations. For each carrier concentration these correlations were monitored as a function of temperature. The details of this study will be discussed extensively in the next section.

IV. NEUTRON DIFFRACTION

A. Introduction

In neutron-diffraction experiments ferromagnetic ordering will result in magnetic Bragg scattering superimposed on the nuclear Bragg reflections below the transition temperature T_c. For a reentrant spin glass the ferromagnetic ordering will also result in increasing Bragg scattering with decreasing temperature, until the transition temperature to the spin-glass state is reached, below which the intensity of the reflection will decrease.[17,29] In the case of an ideal spin-glass state there is no periodic long-range order, so no increase in the Bragg intensity will be observed below the freezing temperature T_f.

Since for the actual Mn concentrations the magnetic intensity will be small compared to the nuclear Bragg intensity, it is necessary to select reflections for which this nuclear intensity is weak. Fortunately, the rocksalt crystal structure of $Sn_{1-x}Mn_xTe$ and the scattering lengths of Sn, Mn, and Te (6.228 fm, -3.73 fm, and 5.80 fm, respectively) offer this possibility. In the rocksalt structure the only Bragg reflections allowed are those with Miller-indices $h,k,l=2n$ and $h,k,l=2n+1$. For the subset with odd indices the nuclear structure factor F_{nucl} equals zero for $x=0.043$. There is no composition for which the other subset of reflections can be suppressed. The reflections with $h,k,l=2n+1$ are obviously the most favorable ones for magnetic studies and, because the magnetic form factor decreases with increasing scattering vector $|\mathbf{Q}|$, especially the (111) reflection.

All neutron-diffraction experiments were performed on $Sn_{0.96}Mn_{0.04}Te$ single crystals. The Mn concentration $x=0.04$ is close enough to 0.043 to reduce the nuclear (111) intensity almost to zero. Except for the as-grown, $p=11\times10^{20}$ cm^{-3} crystal, the samples were the same ones that were used in the measurements of the susceptibility. The sample with $p=11\times10^{20}$ cm^{-3} was from the same Bridgman batch as the other crystals and identical in composition to the sample used for the susceptibility measurements. The experiments were performed on the HB3 triple-axis spectrometer at the high flux reactor Petten. The wavelength of the incident neutrons was 0.1428 nm. Two 30′ Soller collimators were placed between the reactor and the C(002) monochromator and between the sample and the C(002) analyzer, respectively. To suppress second-order reflections a tuned pyrolytic graphite filter was installed between the monochromator

and the sample. With a pair of external Helmholtz coils a magnetic field up to 5.0 mT could be applied perpendicular to the horizontal scattering plane. The lowest temperature that could be reached in the experiments was approximately 1.7 K. For all crystals we studied the profile of the (111) reflection along the [110] direction as a function of temperature. Measurements were performed both with and without the analyzer to examine the presence of inelastic scattering. Moreover, by the installation of the analyzer the contribution of the second-order (222) reflection to the scattered intensity at the (111) position was further reduced. The (222) reflection, for which the magnetic contribution is negligible compared to the nuclear scattering, was also measured at a few temperatures. The purpose of these measurements was twofold. First, it could be checked whether intensity variations in the (111) reflection were indeed of magnetic origin, and not due to structural changes, and, second, an absolute value for the magnetization could be deduced from the relation[30] between the integrated magnetic (111) scattering $I_{\text{magn}}(111)$ and the integrated nuclear (222) scattering $I_{\text{nucl}}(222)$:

$$I_{\text{magn}}(111)=\frac{2}{3}\left[\frac{\gamma e^2}{m_e c^2}\right]^2\langle S\rangle^2 f^2(111)\frac{\sin 2\theta(222)}{\sin 2\theta(111)} \times\frac{16}{F^2_{\text{nucl}}(222)} I_{\text{nucl}}(222)\ . \quad (1)$$

Equation (1) is valid for a multidomain single crystal. The factor $\frac{2}{3}$ results from the averaging over magnetization directions in a cubic structure, assuming that equivalent domain types contain the same number of spins. The magnetic form factor has the value $f(111)=0.815$, $\langle S\rangle$ is the average spin on the Sn/Mn sites, $(\gamma e^2/m_e c^2)=0.539\times 10^{-12}$ cm, $2\theta(111)$ and $2\theta(222)$ are the scattering angles, and $F_{\text{nucl}}(222)$ is the nuclear structure factor for the (222) reflection. Inserting $\langle S\rangle=\frac{5}{2}x$ in Eq. (1) yields the maximum magnetic intensity for a multidomain ferromagnet at zero temperature, i.e., with full alignment of the Mn^{2+} spins within the individual domains.

The measured profiles were fitted with a Gaussian peak shape and a constant background:

$$I=B+I_0\exp\left[-4\ln 2\frac{q^2}{(\text{FWHM})^2}\right]\ . \quad (2)$$

Here q is the distance between the point $Q=(Q_x,Q_x,1)$ and the reciprocal lattice point (1,1,1), when measured along the [110] direction, and FWHM is the full width at half maximum. Besides the analysis of the composite, i.e., magnetic plus nuclear, (111) profile we also performed a detailed study of the separated magnetic (111) reflection. The details of this analysis will be discussed below.

B. Results for $Sn_{0.96}Mn_{0.04}Te$ with $p=7\times 10^{20}$ cm^{-3}

For the Sn-annealed $p=7\times 10^{20}$ cm^{-3} sample the integrated intensity of the Gauss fits to the (111) profile, observed in triple-axis configuration with the analyzer set at zero energy transfer, is presented as a function of temperature in Fig. 5. The variation of the intensity with temperature in double-axis mode is qualitatively similar. In agreement with the results of the ac susceptibility, the magnetization, and the magnetic specific heat, the diffraction data indicate a transition to a ferromagnetically ordered phase with a transition temperature $T_c=6.2\pm 0.1$ K. Below T_c the magnetic intensity is superimposed on the temperature-independent nuclear (111) and second-order (222) intensity. The full line in Fig. 5 represents the result of a mean-field calculation for a three-dimensional ferromagnet with $T_c=6.2$ K and $S=\frac{5}{2}$. The agreement between the data and this curve is excellent. The same mean-field-like temperature dependence of the integrated (111) intensity was found previously[13] for samples of $Sn_{0.97}Mn_{0.03}Te$ with $p=7\times 10^{20}$ cm^{-3} and $Sn_{0.94}Mn_{0.06}Te$ with $p=11\times 10^{20}$ cm^{-3}.

With Eq. (1) a "theoretical" value for the maximum integrated magnetic (111) intensity can be calculated from the measured integrated nuclear (222) intensity. Assuming that the actual Mn concentration is equal to the nominal value $x=0.04$, the observed magnetic (111) intensity (extrapolated to $T=0$ K) amounts to (0.87 ± 0.03) of the calculated value, corresponding to a magnetization of (0.93 ± 0.02) of the theoretical value. Considering the Mn concentration $x=0.044$ deduced from the high-temperature susceptibility, these numbers suggest that the alignment of the spins within the domains is not perfect even at $T=0$ K. By the application of a magnetic field while cooling through T_c the observed magnetic intensity increases: fields of 2.5 and 5.0 mT yield magnetizations of 1.00 and 1.05 times the theoretical value, respectively. This increase must be attributed to the fact that domains with a magnetization component along the field are favored when the domains are formed, meaning

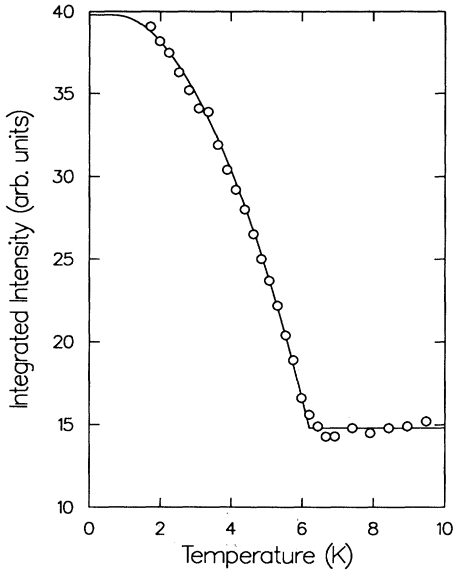

FIG. 5. Temperature dependence of the integrated (111) intensity for $Sn_{0.96}Mn_{0.04}Te$ with $p=7\times 10^{20}$ cm^{-3}, triple-axis mode, $B=0.0$ mT. Full curve: mean-field approximation for $S=\frac{5}{2}$ and $T_c=6.2$ K.

that crystallographically equivalent domains do no longer contain an equal number of spins.

The separate magnetic (111) reflection was obtained by subtracting the nuclear (111) profile, as measured above the transition temperature T_c, from the composite profile observed at temperatures below T_c. At all temperatures below T_c the magnetic (111) reflection can be fitted to a Gaussian profile with a linewidth that is within the experimental accuracy equal to the experimental resolution as determined by the FWHM of the nuclear (111) reflection. This indicates that the ferromagnetic order below the critical temperature is truly long range, and hence the sample is a ferromagnet, albeit with an imperfect alignment of the spins even at $T=0$ K.

C. Results for $Sn_{0.96}Mn_{0.04}Te$ with $p=11\times10^{20}$ cm^{-3}

Figure 6 shows the integrated intensity of the (111) reflection as a function of temperature for the as-grown $p=11\times10^{20}$ cm^{-3} crystal in fields of 0.0, 2.5, and 5.0 mT. For reasons that will become clear below, in this case the integrated intensity has not been determined by fitting the Gaussian profile (2) to the (111) reflection, but by a point-by-point summation over the measured profile. The data in the figure are obtained from the triple-axis experiments with zero energy transfer. Because the measurements in two-axis configuration yielded similar results, we will not discuss them here. It is obvious that, unlike the sample with $p=7\times10^{20}$ cm^{-3}, the temperature dependence of the magnetic intensity in zero field cannot be described with a mean-field prediction. With decreasing temperature the intensity starts to rise at approximately 6.5 K, indicating a transition to a ferromagnetic state, but the increase is more gradual than for $p=7\times10^{20}$ cm^{-3}. The most striking departure from mean-field behavior occurs just above 2 K, where the intensity reaches a maximum at 2.1 K and then decreases with decreasing temperature. The magnetization derived from the maximum observed magnetic intensity in zero field amounts (0.70±0.02) of the theoretical value calculated from the integrated nuclear (222) intensity, assuming the nominal Mn concentration and inserting $\langle S\rangle=\frac{5}{2}x$ in Eq. (1). Applying a 2.5 mT field increases the maximum observed intensity to a value corresponding to a magnetization of (0.76±0.02) times the theoretical value, but, as can be seen in Fig. 6, does not remove the decrease of the intensity below 2.1 K. In a 5.0 mT field no decrease of the magnetic intensity with decreasing temperature is observed in the range down to 1.8 K. The observed magnetic intensity at 1.8 K corresponds to a fraction of (0.80±0.02) of the theoretical magnetization.

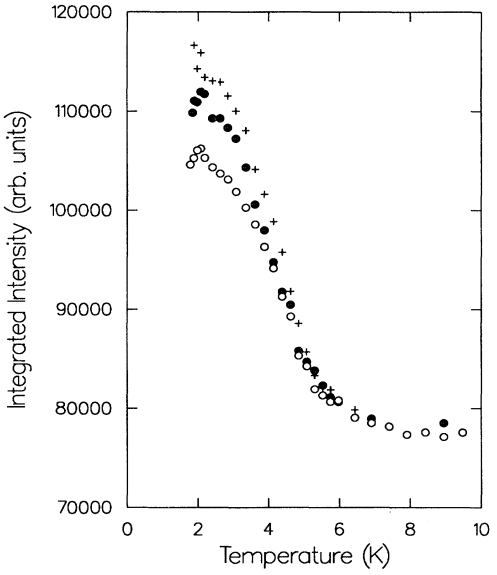

FIG. 6. Temperature dependence of the integrated (111) intensity for $Sn_{0.96}Mn_{0.04}Te$ with $p=11\times10^{20}$ cm^{-3}, triple-axis mode, $B=0.0$ mT (○), $B=2.5$ mT (●), and $B=5.0$ mT (+).

We now turn to the analysis of the separate magnetic (111) profile, again obtained by the subtraction of the nuclear (111) profile, measured at temperatures above 6.5 K, from the composite profiles observed below this temperature. Above 5.5 K the magnetic profiles could not be determined accurately enough to perform meaningful fits. Whereas the nuclear reflection can well be described by the Gaussian profile (2), this is not the case for all magnetic profiles, except those observed at temperatures below 4 K in the 5.0 mT field. For this reason the integrated intensities in Fig. 6 were not determined by Gauss fits to the composite (111) profile, but by point-to-point summation. All magnetic reflections observed in fields of 0.0 and 2.5 mT and those above 4 K in 5.0 mT are significantly broader than the nuclear ones and display non-Gaussian wings that are not present in the nuclear reflections. As an example, Fig. 7 shows the magnetic profile observed at 1.8 K in zero field, together

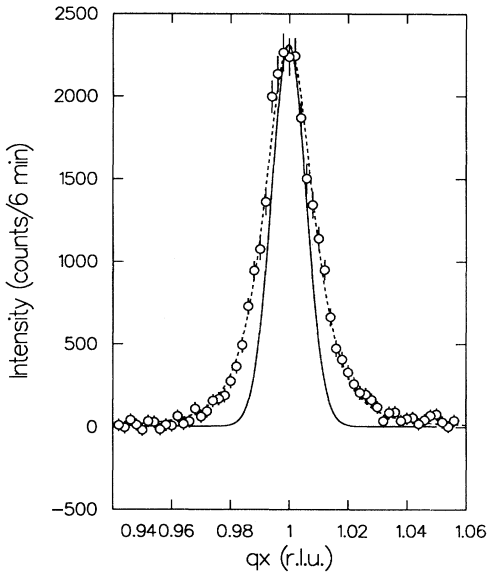

FIG. 7. $Sn_{0.96}Mn_{0.04}Te$, $p=11\times10^{20}$ cm^{-3}, triple-axis mode, $T=1.8$ K, $B=0.0$ mT: magnetic (111) profile along the [110] direction. Dashed curve: fit to a Lorentzian, convoluted with the Gaussian experimental resolution function. Full curve: Gaussian with the width of the experimental resolution function.

with a Gaussian with equal amplitude and with the FWHM of the nuclear (111) reflection. The broad, non-Gaussian profile of the magnetic reflection implies that the ferromagnetic order that sets in below 6.5 K as indicated by the data in Fig. 6 is *not* long ranged. Only in the measurements in 5.0 mT below 4 K the magnetic order cannot be distinguished from true long-range order. In the fields of 0.0 and 2.5 mT long-range order is not established in the temperature range down to 1.8 K.

An alternative description of magnetic intensity profiles resulting from short- or intermediate-range order, is the Lorentzian form

$$I = B + \frac{I_0}{q^2+\kappa^2} , \tag{3}$$

where κ is the half width at half maximum (HWHM). This Lorentzian profile can be attributed to scattering by finite magnetic clusters characterized by a correlation length $1/\kappa$. The experimentally observed profile for scattering with an intrinsic Lorentzian character is determined by the convolution of the Lorentzian with the Gaussian experimental resolution function. Where possible, we fitted the magnetic (111) reflections with a line shape resulting from such convolution. In these fits the FWHM of the Gauss function was fixed at the value determined from the nuclear (111) reflection. This line shape appears to give a good description of the experimental data, as can be seen in Fig. 7 for the data at 1.8 K in zero field. Figure 8 displays the HWHM of the Lorentzian deduced from the fits as a function of temperature. No data are shown for the 5.0 mT field below 4.8 K, because in this temperature range the Lorentzian becomes too narrow ($\kappa < 0.002$ reciprocal lattice units) to perform a successful deconvolution. However, only below 4 K the width of the observed magnetic profile is equal to the experimental resolution, corresponding to $\kappa \equiv 0$ and implying long-range order.

In zero field as well as in fields of 2.5 mT and 5.0 mT κ initially decreases when the temperature is lowered, until it becomes constant near 4 K. In 0.0 and 2.5 mT κ remains finite below 4 K, in 5.0 mT it equals zero. The decrease of κ reflects the increase of the ferromagnetic correlation length, i.e., the growth of ferromagnetically ordered clusters, with decreasing temperature. The fact that at a fixed temperature the value of κ significantly decreases with increasing field, implies that the correlations are drastically enhanced by the application of a field. Below 4 K a field of 5.0 mT appears to be sufficient for the formation of a magnetic cluster of apparently infinite size.

Below 2.5 K κ increases with decreasing temperature in the case of the zero-field measurements. This occurs in the temperature range where the integrated magnetic intensity reaches its maximum. The increasing width of the magnetic reflection implies a decrease of the ferromagnetic correlation length and suggests a transition from a (restricted-range) ferromagnetic order into a spin-glass-like state. Obviously a field as small as 2.5 mT is sufficient to suppress this effect: in this field κ remains more or less constant at the value reached near 4 K, although also in this case the integrated intensity decreases below 2 K. An increase of κ at lower temperatures can therefore not be excluded.

The same temperature dependence of the inverse correlation length as that observed in zero field, also in combination with a decrease of intensity at low temperature, was found by Maletta, Aeppli, and Shapiro[17] in their experiments on $Eu_xSr_{1-x}S$ reentrant spin glasses. This corroborates the conclusion from our susceptibility and magnetization experiments that $Sn_{0.96}Mn_{0.04}Te$ with $p = 11\times10^{20}$ cm^{-3} is a reentrant spin glass. With decreasing temperature first a ferromagnetically ordered state is gradually formed between 6.5 and 4 K, followed by a transition to a spin-glass state between 2.5 and 2.0 K. This interpretation is supported by the agreement between the characteristic temperatures in the behavior of κ in zero field and those for the susceptibility experiments displayed in Fig. 2. The real part of the susceptibility goes through a maximum in the temperature range where κ becomes constant when the temperature is lowered, indicating the ferromagnetic transition, whereas the imaginary part has its maximum where κ starts to increase, indicating the transition to the spin-glass state.

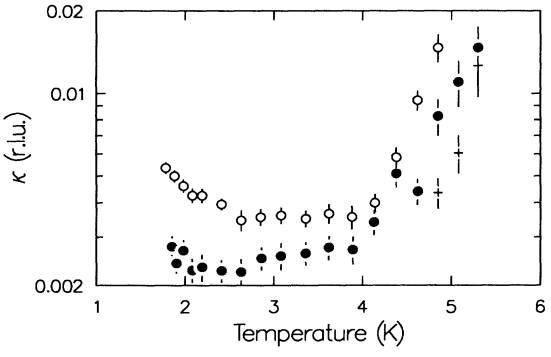

FIG. 8. $Sn_{0.96}Mn_{0.04}Te$, $p = 11\times10^{20}$ cm^{-3}, triple-axis mode: temperature dependence of the inverse correlation length κ, $B = 0.0$ mT (○), $B = 2.5$ mT (●), and $B = 5.0$ mT (+).

D. Results for $Sn_{0.96}Mn_{0.04}Te$ with $p = 23\times10^{20}$ cm^{-3}

In Fig. 9 the scaled integrated intensity for the (111) reflection, obtained by point-by-point summation, is displayed versus temperature for the $Sn_{0.96}Mn_{0.04}Te$ crystal with $p = 23\times10^{20}$ cm^{-3}, together with the corresponding data for the other two samples. The data in the figure are from the triple-axis measurements with zero energy transfer, but the temperature dependence of the integrated intensity in double-axis mode was qualitatively similar. To enable a fair comparison, the intensity has been normalized by subtracting the nuclear scattering observed at temperatures above 6 K and subsequent scaling to the maximum magnetic intensity calculated from the observed nuclear (222) intensity with Eq. (1). The figure shows that below 6 K there is some magnetic (111) intensity present for the crystal with $p = 23\times10^{20}$ cm^{-3}, but that it is much smaller than for the other two samples. The maximum observed magnetic intensity in triple-axis

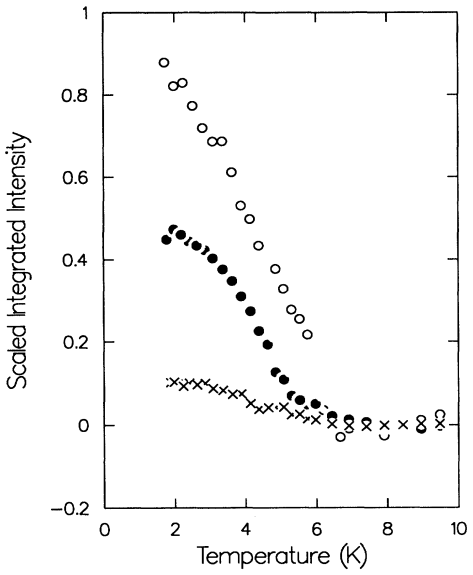

FIG. 9. Temperature dependence of the magnetic (111) intensity, scaled on the maximum magnetic (111) intensity calculated from the nuclear (222) intensity, for $Sn_{0.06}Mn_{0.04}Te$ with $p=7\times10^{20}$ cm^{-3} (○), $p=11\times10^{20}$ cm^{-3} (■), and $p=23\times10^{20}$ cm^{-3} (×). Triple-axis mode, $B=0.0$ mT.

mode amounts to roughly 10% of the value expected from Eq. (1), corresponding to a magnetization of ~0.32 of the theoretical value for $x=0.04$ and $\langle S\rangle=\frac{5}{2}x$. The application of a magnetic field of 5.0 mT had no effect on the observed intensity.

The magnetic intensity is so small that the subtraction procedure to separate the magnetic and the nuclear (111) profiles could not be applied at each individual temperature. As an alternative the magnetic profile at low temperatures was obtained by subtracting the sum of five scans performed between 8 and 10 K from the sum of the five scans performed below 2.2 K. Figures 10(a) and 10(b) show the results for the double- and triple-axis measurements, respectively. In both cases the magnetic profile does clearly not have a Gaussian form, in contrast to the nuclear (111) Bragg reflection, of which the FWHM is indicated in the figure.

A comparison between the Figs. 10(a) and 10(b) indicates that for this sample there is a difference between the double- and triple-axis magnetic profiles. The profile observed in triple-axis configuration appears to be much more diffuse than that from the double-axis measurements. In the latter case there obviously is a considerable contribution to the scattered intensity from inelastic processes, which cause the sharp peak superposed on the very broad distribution from (quasi)elastic processes. By the installation of the analyzer, which allows the observation of neutrons scattered with an energy change $\Delta E<1.5$ meV only, this contribution is removed. An attempt to determine a characteristic energy of the inelastic processes did not succeed. Although the diffuse character of the magnetic scattering is somewhat less pronounced in the double-axis measurements, both in the double- as well as in the triple-axis mode the distribution in Q-space of the magnetic (111) scattering is more diffuse than that of the nuclear (111) scattering. This implies that the ferromagnetic correlations in real space have a short-range character. The correlations are gradually built up below 6 K, resulting in the increase in intensity depicted in Fig. 9. Because of the short-range character, we believe that the observation of magnetic intensity in zero field at the nuclear (111) Bragg position does not violate the conclusion from the measurements of the susceptibility, the magnetization, and the specific heat that

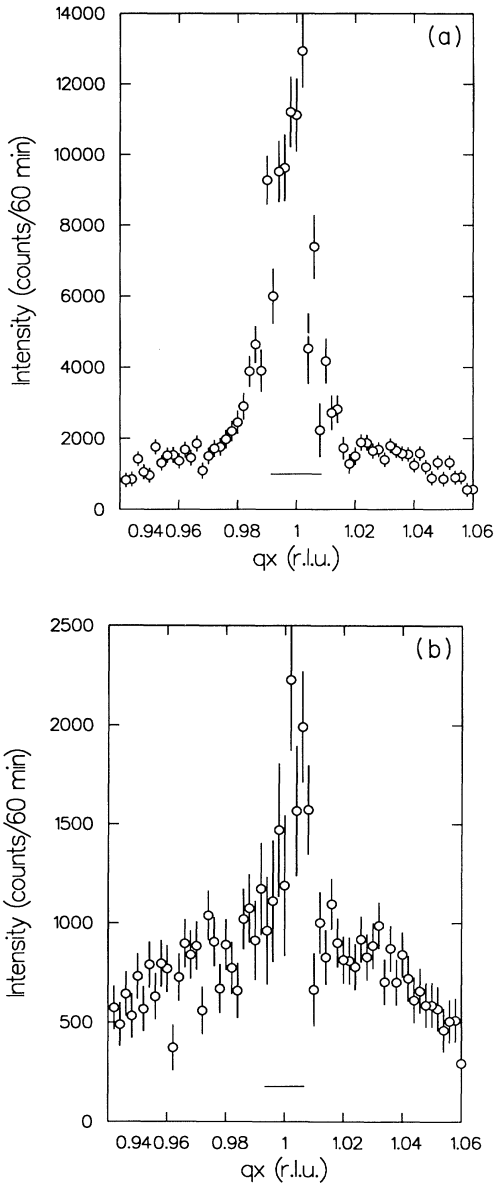

FIG. 10. $Sn_{0.96}Mn_{0.04}Te$, $p=23\times10^{20}$ cm^{-3}: magnetic (111) profile along the [110] direction at $T\approx2$ K, (a) double-axis mode, (b) triple-axis mode. Horizontal lines represent the experimental resolutions (FWHM).

the low-temperature phase for this combination of Mn concentration and charge-carrier concentration is a spin-glass state. In fact, in a real spin glass, containing a few percent solute magnetic atoms, the presence of short-range magnetic correlations is inevitable, even if the positional randomness of the magnetic and nonmagnetic atoms is complete.[31]

The temperature below which the scattered intensity increases, approximately 6 K, may be regarded as the freezing temperature corresponding to the time constant ($\sim 3\times10^{-12}$ s), determined by the energy window $\Delta E = 1.5$ meV. Spins which are not frozen, but are involved in a relaxation process with a time constant $\tau > 3\times10^{-12}$ s, contribute to the quasielastic scattering and are indistinguishable from frozen spins, for which $\tau \rightarrow \infty$. Because of the different time constant ($\sim 10^{-3}$ s), the susceptibility measurements yield a different freezing temperature. A similar dependence of the apparent freezing temperature on the characteristic time constant of the measurement was reported by Murani and Heidemann[31] for a *Cu*Mn spin glass.

V. DISCUSSION

We have presented experimental evidence for the existence of a transition from a ferromagnetic state into a spin-glass phase in the diluted magnetic semiconductor $Sn_{0.96}Mn_{0.04}Te$, induced by an increase in the charge-carrier concentration alone. The breakdown of the long-range ferromagnetically ordered state, observed in the sample with $p = 7\times10^{20}$ cm^{-3}, with increasing carrier density is a gradual process: in the sample with $p = 11\times10^{20}$ cm^{-3} initially a limited-range ferromagnetic order is established with decreasing temperature, but when the temperature is lowered further this order collapses and a reentrant spin-glass phase is entered. For the sample with $p = 23\times10^{20}$ cm^{-3} a direct transition from the paramagnetic regime into a spin-glass state occurs.

Because the Curie-Weiss temperature Θ remains constant when the charge-carrier concentration is increased, the breakdown of the ferromagnetic state is apparently not caused by a change in the total interaction strength. In that respect this transition is different from that occurring at $p_c = 3\times10^{20}$ cm^{-3}, where the ferromagnetism is so to say switched on. Both the rise of Θ at p_c and the p independence of Θ for $p \geq 7\times10^{20}$ cm^{-3} are in agreement with calculations based on the RKKY model described in the Introduction of this paper.[11]

With the assumption of RKKY interactions between the magnetic moments it is also possible to understand the carrier-concentration-induced transition between a ferromagnetic state and a spin-glass state.[15] The RKKY interaction is a rapidly oscillating function with argument $2k_F R_{ij}$, where $k_F (\sim p^{1/3})$ is the Fermi wave vector and R_{ij} is the distance between the magnetic ions. For $2k_F R_{ij} \rightarrow 0$ the interaction is ferromagnetic. Two characteristic distances can be distinguished. The first, R_0, is the distance at which the first change from ferromagnetic to antiferromagnetic interactions occurs. At a fixed Mn concentration R_0 depends on the carrier concentration as $R_0 \sim p^{-1/3}$. The second, $R_{\text{Mn-Mn}}$, is the average spin-spin distance and depends on the Mn concentration as $R_{\text{Mn-Mn}} \sim x^{-1/3}$. The ratio between $R_{\text{Mn-Mn}}$ and R_0, or equivalently p and x, is of crucial importance for the magnetic behavior. If $R_0 \ll R_{\text{Mn-Mn}}$ there is a competition between positive, ferromagnetic interactions and negative, antiferromagnetic interactions, leading to the formation of a spin-glass state. Because of their high carrier concentrations ($\sim 10^{23}$ cm^{-3}) this is the case in canonical metallic spin glasses such as *Cu*Mn. If $R_0 \gg R_{\text{Mn-Mn}}$ ferromagnetic interactions dominate and no spin-glass phase will be formed, but a ferromagnetically ordered state. In $Sn_{1-x}Mn_xTe$, with x and p in the range of the samples discussed in this paper, the situation is intermediate between these two extremes. R_0 and $R_{\text{Mn-Mn}}$ are of comparable magnitude and a relatively small decrease of R_0, induced by an increase in the charge-carrier concentration, can lead to the observed collapse of ferromagnetism. In systems like *Ag*Fe and *Au*Fe a transition between a ferromagnetic state and a spin-glass state with an intermediate reentrant spin-glass phase has been observed also,[25] but in all these cases transitions were induced by decreasing the concentration of the magnetic ions and thus increasing $R_{\text{Mn-Mn}}$ instead of decreasing R_0.

The delicate interplay between the Mn concentration and the charge-carrier concentration is illustrated in Fig. 11. The Curie-Weiss temperature Θ and the temperature $T_{\max}$, where the real part of the ac susceptibility has its maximum, both scaled on x (in % Mn), are plotted versus the carrier concentration in the Σ band p_Σ, also scaled on x. We have chosen to plot the objective quantity $T_{\max}$ instead of the critical temperature T_c and/or the freezing

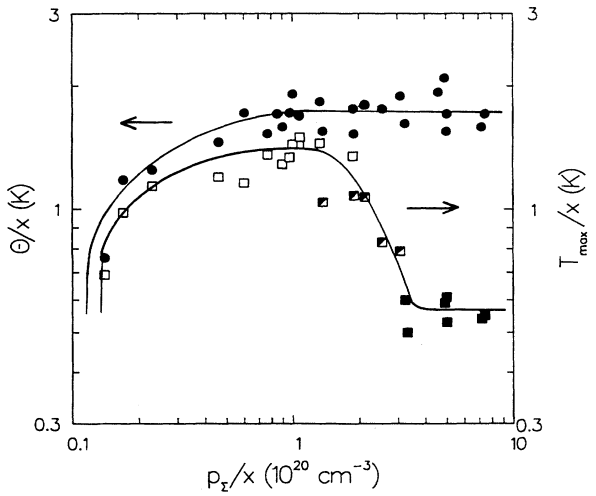

FIG. 11. $Sn_{1-x}Mn_xTe$, $0.02 \leq x \leq 0.10$: Curie-Weiss temperature Θ (●) and the temperature $T_{\max}$ (squares), where the real component of the ac susceptibility has its maximum, both scaled on the Mn concentration x (expressed in % Mn), vs the charge-carrier concentration in the Σ band p_Σ, also scaled on x. Open squares: ferromagnet; semi-filled squares: reentrant spin glass; filled squares: spin glass. The lines are guides to the eye.

temperature T_f to avoid errors because of a possible misinterpretation of the experimental data. The measured carrier concentration p has been replaced by $p_\Sigma = p - p_c = p - 3\times10^{20}$ cm^{-3}, because, as described in the Introduction, the contribution to the RKKY interaction by the holes from the light-hole band is negligible compared to that by those from the heavy-hole Σ band.[10] Data are included for compositions with $0.02 \le x \le 0.10$ and carrier concentrations 3×10^{20} cm$^{-3} \le p \le 23\times10^{20}$ cm^{-3}. The figure shows that Θ/x is more or less constant at $\Theta/x = 1.75$ for $p_\Sigma/x \ge 0.5$. For $p_\Sigma/x \le 0.5$ a part of the steplike increase of Θ at $p = p_c$ can be seen. In the T_{max}/x data four regimes can be distinguished: (I) for $p_\Sigma/x \le 0.5$ the ferromagnetic state is formed in accordance with the increase in Θ/x; (II) for $0.5 \le p_\Sigma/x \le 1.5$ a long-range-ordered ferromagnetic phase is formed, identified by a maximum in the susceptibility at $T_{max}/x \approx 1.5$; (III) for $1.5 \le p_\Sigma/x \le 3.0$ an initial transition from the paramagnetic state to a state with a ferromagnetic order of restricted range is followed by a transition to a spin-glass phase at lower temperature. The ferromagnetic transition is characterized by a maximum in the susceptibility at T_{max}, with $1.5 \ge T_{max}/x \ge 0.6$. T_{max}/x decreases with increasing p_Σ/x. (IV) For $p_\Sigma/x \ge 3.0$ a spin-glass state is formed, directly from the paramagnetic state, at the freezing temperature $T_f/x = T_{max}/x \approx 0.6$. The data in Fig. 11 corroborate the decisive role in the low-temperature magnetic behavior of the ratio p_Σ/x and supports the assumption of RKKY-like interactions.

For the reentrant spin-glass systems the transition temperature T_f to the spin-glass phase, denoted by a maximum in the imaginary part of the susceptibility, is not included in Fig. 11. Up till now a reentrant phase has been observed in samples with $x = 0.03$, 0.04, and 0.05 with $p \approx 10\times10^{20}$ cm^{-3} and $x = 0.08$ with $p \approx 20\times10^{20}$ cm^{-3}. The data indicate that T_f/x is in the range 0.4–0.7, but do not show a clear trend with p_Σ/x. This is also reflected in Fig. 12, where we present a tentative three-dimensional (T,x,p) magnetic phase diagram. If a cross section for a fixed charge carrier concentration is made, a (T,x) phase diagram is obtained which is similar to that reported by Mauger and Escorne.[14] However, they did not fully recognize the role of the carrier concentration. Three phases can be distinguished in such a (T,x) diagram: the paramagnetic, the ferromagnetic, and the spin-glass phase. These phases meet in a triple point, which shifts towards higher x and higher T with increasing p. The exact shape of the boundary between the ferromagnetic and the spin-glass phase, denoting the reentrant spin-glass transition, is not yet clear. The available data indicate that, starting from the triple point, towards higher x an initially rather flat behavior is followed by a steep decline towards $T = 0$ K.

Of course the diagram in Fig. 12 is still far from complete. Along the x axis an extension is possible in both directions. More experiments on samples with $x \le 0.02$ could elucidate how the lower limit in x for the existence of a ferromagnetically ordered state depends on p. Mn concentrations below $x = 0.03$, however, must be considered as too small for neutron-scattering experiments. For samples with $x \ge 0.10$ an increasing role of direct antiferromagnetic Mn-Mn interactions may be expected to influence the magnetic behavior. Besides the extensions to lower and higher x it is also necessary to obtain more detail in the interval $0.02 \le 0.10$. Especially for $x \ge 0.06$ with $p \approx 20\times10^{20}$ cm^{-3} data are scarce.

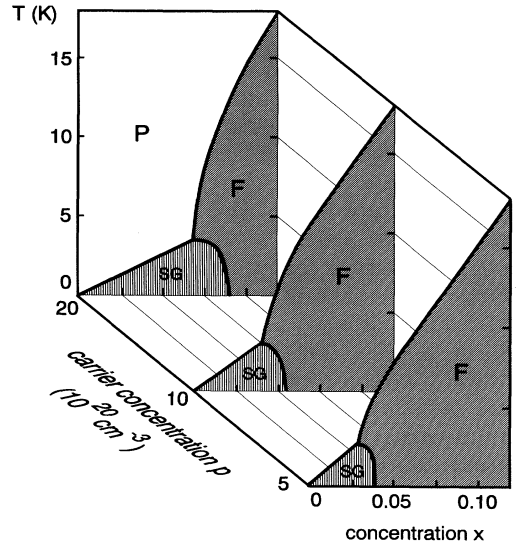

FIG. 12. Three-dimensional (T,x,p) magnetic phase diagram for $Sn_{1-x}Mn_xTe$. P=paramagnetic phase, F=ferromagnetic phase, SG=spin-glass phase.

Along the p axis there is a lack of data in the range 11×10^{20} cm$^{-3} \le p \le 20\times10^{20}$ cm^{-3}. Measurements on samples with carrier concentrations in this range are essential to study the gradual breakdown of ferromagnetism with increasing p at fixed x. However, thus far it has been difficult to precisely control the isothermal annealing process. It is not yet possible to tune the annealing parameters in such a way that every desired carrier concentration can be achieved. Variation of the annealing temperature and/or the source material are possibilities to reach carrier concentrations other than $5–7\times10^{20}$ cm^{-3} or $20–23\times10^{20}$ cm^{-3}. For example, using Zn as source material yields carrier concentrations below p_c. Instead of annealing, it might also be possible to *grow* material with a carrier concentration different from $9–11\times10^{20}$ cm^{-3}. According to the Sn-Te phase diagram[16] another cation-anion ratio in the starting materials should lead to another carrier concentration. Another possibility is the replacement in the starting materials of a few percent Sn by an element with a valency other than +2. First experiments with 3% In as dopant in material with 3% Mn yielded lower carrier concentrations than in undoped 3% Mn samples, but there are indications that the magnetic properties are also changed in comparison to undoped $Sn_{0.97}Mn_{0.03}Te$ with the same carrier concentration.

The extension of the magnetic phase diagram towards temperatures below 1.3 K is essential to establish the exact position of both boundaries of the spin-glass regime. Concerning the neutron-scattering experiments, especial-

ly for the $Sn_{0.96}Mn_{0.04}Te$ crystal with $p=11\times10^{20}$ cm^{-3} measurements below 1.8 K would be interesting. In zero field the further decrease of the size of the ferromagnetically ordered clusters could be followed, which might eventually lead to results similar to those found in the present experiments on the sample with $p=23\times10^{20}$ cm^{-3}. The effect of the magnetic field should be studied in more detail. Measurements in a field of 2.5 mT could reveal whether in this field the observed decrease in intensity is also accompanied by a decrease in correlation length, starting at lower temperature in comparison to the zero-field case. A decrease in intensity at low temperatures can also not be excluded in the 5.0 mT field. This actually implies the extension of the three-dimensional (T,x,p) phase diagram to a four-dimensional (T,x,p,B) phase diagram. Besides neutron-scattering experiments, also magnetization measurements, both field cooled and zero field cooled, in different fields can contribute to the compilation of such a diagram. For the crystal with $p=23\times10^{20}$ cm^{-3} inelastic-neutron-scattering experiments with a better energy resolution might clarify the nature of the fluctuation processes that cause the observed difference between the double- and triple-axis measurements.

A problem that remains to be solved is the reduction of the magnetic moment for the ferromagnetic samples, that is calculated from the neutron-scattering data with Eq. (1). This reduction has not only been observed for $Sn_{0.96}Mn_{0.04}Te$ with $p=7\times10^{20}$ cm^{-3} (93% of the theoretical magnetization is observed), but also for $Sn_{0.94}Mn_{0.06}Te$ with $p=11\times10^{20}$ cm^{-3} (75%) and $Sn_{0.90}Mn_{0.10}Te$ with $p=11\times10^{20}$ cm^{-3} (79%).[13] Preliminary high-field (up to 7 T) magnetization measurements on the two latter samples confirm this reduction: in both cases the measurements yield a saturation magnetization corresponding to approximately 85% of the value that is expected assuming the nominal Mn concentration and $\langle S\rangle=\frac{5}{2}$. It is not yet clear whether the reduction of the magnetization is caused by a reduction of the magnetic moment of each individual Mn ion or by the existence of groups of antiferromagnetically coupled Mn ions that persist down to $T=0$ K as isolated regions within an infinitely sized ferromagnetic cluster.

A complete, both qualitatively and quantitatively satisfactory theoretical description of the phenomenon of the carrier-concentration-induced breakdown of the ferromagnetic state is not yet available. Such description can possibly be supplied by a model in terms of clusters and random fields, as was used, for example, for $(Fe_xMn_{1-x})_{75}P_{16}B_6Al_3$ (Ref. 32) and $Eu_xSr_{1-x}S$.[33] Especially for the sample with $p=11\times10^{20}$ cm^{-3} the large effect of small applied magnetic fields on the ferromagnetic correlation length suggests that a random-field model might be appropriate. In this model a random field is imposed on ferromagnetically ordered clusters by spins that are not included in such a cluster, which leads to reentrant spin-glass behavior. The effect of the random field can be eliminated by the application of a small external field, resulting in the persistence of the ferromagnetic state down to $T=0$ K.

ACKNOWLEDGMENTS

We would like to thank Dr. T. Story for helpful discussions and A. Bontenbal, M. G. van Opstal, M. M. H. Willekens, A. G. Menting, M. A. M. Haast, C. van der Steen, H. J. M. Heyligers, and J. Johansson for their experimental assistance, Dr. A. G. Schins is acknowledged for providing the deconvolution program. The research of Dr. Swagten is made possible by financial support from the Royal Netherlands Academy of Arts and Sciences.

[1]J. K. Furdyna, J. Appl. Phys. **64**, R29 (1988).
[2]W. J. M. de Jonge and H. J. M. Swagten, J. Magn. Magn. Mater. **100**, 323 (1991).
[3]M. Escorne, A. Mauger, J. L. Tholence, and R. Triboulet, Phys. Rev. B **29**, 6306 (1984).
[4]M. Mathur, D. Deis, C. Jones, A. Patterson, W. Carr, and R. Miller, J. Appl. Phys. **41**, 1005 (1970).
[5]U. Sondermann, J. Magn. Magn. Mater. **2**, 216 (1976).
[6]M. Inoue, M. Tanabe, H. Yagi, and T. Tatsukawa, J. Phys. Soc. Jpn. **49**, 835 (1980).
[7]R. W. Cochrane, F. T. Hedgcock, and J. O. Strom-Olsen, Phys. Rev. B **9**, 3013 (1974).
[8]M. Rudermann and C. Kittel, Phys. Rev. **96**, 99 (1954); T. Kasuya, Prog. Theor. Phys. **16**, 45 (1956); K. Yosida, Phys. Rev. **106**, 893 (1957).
[9]T. Story, R. R. Galązka, R. B. Frankel, and P. A. Wolff, Phys. Rev. Lett. **56**, 777 (1986).
[10]H. J. M. Swagten, W. J. M. de Jonge, R. R. Galazka, P. Warmenbol, and J. T. Devreese, Phys. Rev. B **37**, 9907 (1988).
[11]T. Story, P. J. T. Eggenkamp, C. H. W. Swüste, H. J. M. Swagten, W. J. M. de Jonge, and L. F. Lemmens, Phys. Rev. B **45**, 1660 (1992).
[12]W. J. M. de Jonge, H. J. M. Swagten, S. J. E. A. Eltink, and N. M. J. Stoffels, Semicond. Sci. Technol. **5**, S131 (1990).
[13]C. W. H. M. Vennix, E. Frikkee, H. J. M. Swagten, K. Kopinga, and W. J. M. de Jonge, J. Appl. Phys. **69**, 6025 (1991).
[14]A. Mauger and M. Escorne, Phys. Rev. B **35**, 1902 (1987).
[15]W. J. M. de Jonge, T. Story, H. J. M. Swagten, and P. J. T. Eggenkamp, Europhys. Lett. **17**, 631 (1992).
[16]R. F. Brebick, J. Phys. Chem. Solids **24**, 27 (1963).
[17]H. Maletta, G. Aeppli, and S. M. Shapiro, J. Magn. Magn. Mater. **31-34**, 1367 (1983).
[18]H. Kunkel, R. M. Roshiko, W. Ruan, and G. Williams, Philos. Mag. B **64**, 153 (1991).
[19]B. H. Verbeek, G. J. Nieuwenhuys, H. Stocker, and J. A. Mydosh, Phys. Rev. Lett. **40**, 586 (1978).
[20]R. B. Goldfarb, F. R. Fickett, K. V. Rao, and H. S. Chen, J. Appl. Phys. **53**, 7687 (1982).
[21]V. Cannella and J. A. Mydosh, Phys. Rev. B **6**, 4420 (1972).
[22]A. F. J. Morgownik and J. A. Mydosh, Phys. Rev. B **24**, 5277 (1981).
[23]P. J. T. Eggenkamp and C. W. H. M. Vennix (unpublished).
[24]C. Y. Huang, J. Magn. Magn. Mater. **51**, 1 (1985).
[25]G. J. Nieuwenhuys, B. J. Verbeek, and J. A. Mydosh, J. Appl. Phys. **50**, 1685 (1979).
[26]L. E. Wenger and P. H. Keesom, Phys. Rev. B **13**, 4053 (1976).

[27]D. L. Martin, Phys. Rev. B **21**, 1906 (1980).
[28]B. M. Boerstoel, J. J. Zwart, and J. Hansen, Physica **57**, 397 (1972).
[29]H. Maletta and P. Convert, Phys. Rev. Lett. **42**, 108 (1979).
[30]W. Marshall and S. W. Lovesey, *Theory of Thermal Neutron Scattering* (Oxford University Press, London, 1971).
[31]A. P. Murani and A. Heidemann, Phys. Rev. Lett. **41**, 1402 (1978).
[32]G. Aeppli, S. M. Shapiro, R. J. Birgeneau, and H. S. Chen, Phys. Rev. B **28**, 5160 (1983).
[33]H. Maletta, G. Aeppli, and S. M. Shapiro, Phys. Rev. Lett. **48**, 1490 (1982).